Investigation of the Mechanism of Grout Penetration in Intersected Fractures

Yanxu Guo[1], Peng Zhao[2], Qingsong Zhang[1], Rentai Liu[1, *], Lianzhen Zhang[3] and Yankai Liu[1]

Abstract: To study the penetration mechanism of cement-based slurry in intersected fractures during grouting and the related pressure distribution, we have used two different variants of cement, namely, basic cement slurry and fast-setting cement slurry. The influence of a retarder, time-varying viscosity, fracture width and location of injection hole is also considered. A finite element software is used to implement two and three-dimensional numerical models for grouting of intersected fractures in hydrostatic conditions. Results show that there are significant differences in the diffusion morphology and pressure distribution depending on the considered cement slurry. Retarder can effectively slow down the rising rate of injection pressure and extend the diffusion distance of grout. The influence of the branch fracture is more important when basic cement slurry is considered, indicating that the change of grout pressure is correlated with the slurry viscosity. The faster the viscosity increases, the less evident is the effect.

Keywords: Fracture grouting, numerical investigation, intersected fractures, mechanism of grout penetration.

1 Introduction

In the process of tunnel construction, it is highly probable that some unfavorable geological conditions would be encountered, such as water-rich fault fracture zone, jointed and fractured rock mass and so on, which can easily lead to geological hazards such as collapse, water inrush and mud gush under the influence of engineering disturbance or in situ stress. As a commonly used technology in preventing and controlling unfavorable geological hazards in underground engineering, grouting plays an important role in sealing fracture, improving the strength and stability of surrounding rock, and ensuring the construction safety, thus benefiting the subsequent tunnel operation and maintenance.

Because of the complexity and variability of internal structure of fractured rock mass, it is difficult to develop grouting theory. At present, many scholars at home and abroad have carried out a lot of theoretical and experimental research on fracture grouting under

[1] Geotechnical and Structural Engineering Research Center， Shandong University, Jinan, 250061, China.

[2] Powerchina Huadong Engineering Corporation Limited, Hangzhou, 311122, China.

[3] College of Pipeline and Civil Engineering, China University of Petroleum, Qingdao, 266580, China.

[*] Corresponding Author: Rentai Liu. Email: rentailiu@163.com.

various conditions. As for Newtonian fluid, Baker [Baker (1955)] obtained the formula for laminar grout flow within horizontal smooth fracture. Wallner [Wallner (1976)] carried out experiments on the diffusion of Bingham slurry in fractured media and proposed a method for calculating the penetration radius of grout slurry. Based on the work of Wallner, Dai et al. [Dai and Bird (1981)] derived the formula for flow of Bingham slurry within fracture channel with parallel plates, then, Deere and Lombardi (1985), Amadei et al. [Amadei and Savage (2001)] obtained the flow equation for Bingham flow within a single fracture. Li et al. [Li, Huang and Liang (2008)] used elliptical fracture permeation grouting simulation test device to investigate the effects of fracture width, grouting pressure, water cement ratio and grouting time on the diffusion distance and grout volume. Li et al. [Li, Zhang and Zhang (2011)] carried out a model test for grouting of single fracture with flowing water and explored the mechanism of grout penetration and fracture sealing. Zhang et al. [Zhang, Zhang and Liu (2015)] revealed the asymmetric ellipse (AE) diffusion law of the diffusion process of C-S grouting in fissure dynamic grouting based on the experimental conditions by carrying out the model test of cement-water glass (C-S) grouting in a single-plate fracture.

Most of the abovementioned studies assume that the fracture is a parallel plate model, whereas there are many interconnected cracks in the practical fractured rock mass. The crisscross structure of rock fracture plays a decisive role in the diffusion patterns of slurry in the fracture. For this special fracture network, Yang et al. [Yang (2000); Yang, He and Chen (2001)] carried out experimental simulation of grout penetration in fractured rock mass. The general mechanism of grout penetration in fractured rock mass was analyzed and summarized, and the impact factors of grout penetration were discussed. Gothall et al. [Gothall and Stille (2009), Gothall and Stille (2010)] discussed the effect of fracture jacking during grouting and analyzed the interaction between fractures. Based on the three-dimensional geometry and hydraulic characteristics of natural fracture network, Carter et al. [Carter, Dershowitz and Shuttle (2012)] put forward the method of Aperture Controlled Grouting (ACG).

Grout penetration in fractured rock mass is a very complex process. Pure theoretical analysis and experiment cannot dynamically display the diffusion process of the slurry, for lacking direct visualization. Nevertheless, numerical simulation, as an indispensable tool for grouting research, can not only give the results under specific grouting conditions, but also present the process of slurry diffusion continuously and dynamically. Hässler et al. [Hässler, Håkansson and Stille (1992)] took the lead in using numerical simulation to study characteristics of both Bingham and Newtonian grout flow in two-dimensional fracture network. Considering the effect of slurry filtration and the variation of fracture aperture, Eriksson et al. [Eriksson, Stille and Andersson (1992)] discussed the slurry diffusion problem. By developing a grouting model with random fracture network based on Monte-Carlo method, Luo et al. [Luo, Zhu and Huang (2006)] studied the mechanism of grout penetration in rock fracture network and the influence of fracture deformation during the grouting process. Yang et al. [Yang and Sun (2015)] made an attempt to simulate the diffusion behavior of cement slurry in a single fracture by FEM method. By building the Bingham slurry model for grouting of two-dimensional orthogonal fracture network and using the central finite volume method, Wang et al. [Wang, Feng and Wang (2016)] explored the range of slurry diffusion in the fracture under different parameters, thus deriving the formulas concerning grouting diffusion radius and grout volume considering the influence of many factors. Hao et al. [Hao, Wang and Li (2017)] developed a numerical simulation of polymer grout diffusion in a single fracture to analyze the pressure distribution. Kim et al. [Kim, Lee and Yazdani (2018)] used UDEC to simulate the flow of Bingham grout in a single joint with smooth parallel surfaces and considered the hydromechanical coupling to study its effect on grouting performance.

Regarding the difference between the gel characteristics of cement slurry and fast-setting cement slurry, the influence of retarder and the time-varying viscosity of slurry are considered in this paper. The finite element software COMSOL Multiphysics is used to develop a numerical model of two and three-dimensional intersected fractures for simulating grouting diffusion under hydrostatic condition. The mechanism of grout penetration and pressure distribution under hydrostatic condition are investigated, and the influence of time-varying viscosity, fracture width and location of injection hole is analyzed. The paper investigated the mechanism of dynamic grout penetration under hydrostatic condition based on numerical simulation, to provide some guidance and reference for grouting theory and engineering design and practice.

2 Testing of time-varying viscosity of grout

2.1 Test materials

42.5R ordinary Portland cement, water glass and phosphate retarder are used as test materials, where the density, modulus, and concentration of water glass are 1.35 g/cm^3, 3.0, and 37.5 °Bé, respectively. Phosphate retarder is anhydrous sodium dihydrogen phosphate, white solid powder, and its density is 1.949 g/cm^3.

2.2 Test process

(1) The time-varying property test is conducted using the Japanese SV-100 sine wave vibration viscometer. The measurement range is 1~120 Pa·s, and the precision for repeated measurement is 1%.

(2) The water cement ratio is 1:1 and 1.2:1, the volume ratio of cement slurry and water glass mixture (cement slurry volume/water glass volume) is 1:1, 2:1, 3:1, and various groups of experiments are designed and conducted. The retarder is added to groups with volume ratio of the mixture 2:1 and 3:1, where to the corresponding water cement ratio are 1: 1 and 1.2: 1. The cement weight of each group is 100 g, and the retarder is 2% of cement weight.

(3) After mixing with additives, the cement slurry is stirred at the same speed for 3 s, then poured into the instrument. The viscosity and temperature of the mixed slurry is measured once every second, the measured data is stored, and the process with morphological changes after mixing is observed and recorded.

2.3 Time-varying viscosity of grout

According to the test results [Zhao, Zhang and Zheng (2016)], the data about time-varying viscosity are processed with curve fitting. The fitting equation is presented in Tab. 1, and the comparison between fitting curve and experimental data is shown in Figs. 1 and 2, where μ1~μ10 denote the equations for various fitting curves, and μ1'~μ10' represents the test data. The fitting equation can well reflect the time-varying viscosity of slurry, which provides the basis for the subsequent numerical calculation and theoretical study.

Table 1: Equation for time-varying viscosity

Grout type	Water cement ratio	mixture volume ratio	Equation for time-varying viscosity
Cement-water glass slurry	1:1	1:1	$\mu1=0.00240703t^3-0.05890892t^2+1.14539383t-2.86461943$
		2:1	$\mu2=0.00291896t^3+0.02705269t^2+0.2783313t+0.00167993$
		3:1	$\mu3=0.00935071t^3+0.64028509t^2-2.44233531t+3.41789216$
	1.2:1	1:1	$\mu4=0.00053674t^3-0.02833086t^2+0.66904111t-1.55837696$
		2:1	$\mu5=0.00016925t^3+0.01109761t^2+0.49132118t-1.66966132$
		3:1	$\mu6=0.00035680t^3-0.00918743t^2+1.53200906t-4.41093097$
Cement-water glass slurry with retarder	1:1	2:1	$\mu7=0.00000096t^3-0.00078901t^2+0.26763018t+2.08222155$
		3:1	$\mu8=0.00000717t^3-0.00220050t^2+0.37605697t+2.98690275$
	1.2:1	2:1	$\mu9=0.00000041t^3-0.00027142t^2+0.09038338t+1.41892707$
		3:1	$\mu10=0.00001230t^3-0.00451743t^2+0.60918954t+0.29181159$

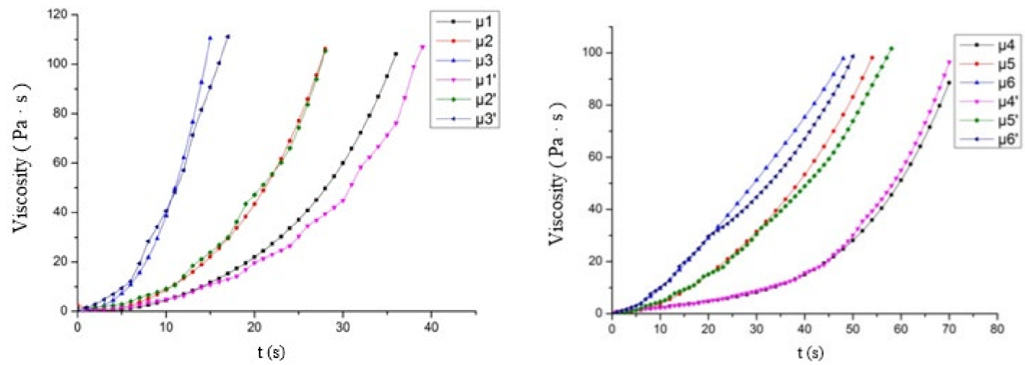

W/C=1:1 W/C=1.2:1

Figure 1: Time-varying viscosity of cement-water glass slurry: comparison between fitting curve and experimental data

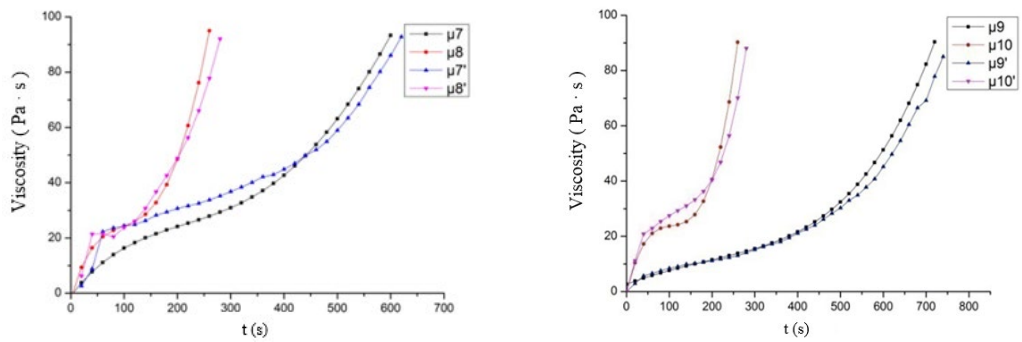

W/C=1:1 W/C=1.2:1

Figure 2: Time-varying viscosity of cement-water glass slurry with retarder: comparison between fitting curve and experimental data

Cement-water glass slurry gelation process without phosphate retarder: When the viscosity is lower than 20 Pa·s, the slurry gelation reaction is incomplete, the viscosity increases slowly, the slurry appearance is liquid, and the fluidity is strong. When the viscosity is higher than 20 Pa·s but lower than 100 Pa·s, the viscosity increases rapidly, the appearance of slurry is solid-liquid mixed paste, and the liquidity is lost rapidly. After the viscosity is higher than 100 Pa·s, the viscosity of the slurry has exceeded the maximum value of the instrument. The measured viscosity value has lost its practical significance. The appearance of the slurry is creamy and has lost fluidity.

The viscosity of cement glass slurry changed significantly with time after adding phosphate retarder: In the initial stage, the gelation reaction is incomplete, and the influence of the slurry is relatively low, the viscosity growth rate is slightly slower than that without adding retarders, the slurry appearance is liquid and fluidity. Then the slurry viscosity remains stable below 40 Pa·s for a long time, and the viscosity growth rate is slow at the beginning, and then gradually increased. The slurry is a solid-liquid mixed paste, which has a certain fluidity. Then the slurry viscosity keeps rising, and its appearance is pasty and has lost fluidity.

The results show that the phosphate retarder has a significant effect on the time-varying viscosity of cement-water glass slurry. The retarder can help reduce the hydration rate of cement and delay the gelation process of slurry, thus making the slurry viscosity below 40 Pa·s for a long time.

3 Numerical investigation of grout penetration in two-dimensional intersected fractures

Based on finite element method, COMSOL Multiphysics is used to simulate real physical phenomena by solving partial differential equation(s). In this paper, the fluid dynamics module is used for numerical simulation. The slurry and water are taken as two types of fluids respectively, and the model for grouting of intersected fractures is established and solved based on the motion control equation of two-phase flow. The level set method is used to trace the interface between slurry and water, and the distribution of slurry and water in the whole area is characterized by volume fraction method. After analyzing some important parameters, including the shape of slurry diffusion, variation of grouting pressure and the distribution of pressure field in the model, the mechanism of grout penetration in intersected fracture model can be obtained.

The motion of the grout in the fracture space follows the N-S equation:

$$\rho\frac{\partial\vec{u}}{\partial t}+\rho(\vec{u}\cdot\nabla)\cdot\vec{u}=\nabla\cdot\left[-pI+\mu(\nabla\vec{u}+(\nabla\vec{u})^T)\right]+\rho\vec{g}+\vec{F} \tag{1}$$

The compressibility of grouting material and groundwater is very small and can be neglected under the current variation range of grouting pressure, so the flow of slurry and groundwater satisfies the continuous equation:

$$\nabla\cdot\vec{u}=0 \tag{2}$$

In the process of grout spreading, there is a mixing zone between slurry and groundwater. To facilitate research and analysis, volume fraction method is used to characterize the motion of the interface between slurry and water. The governing equation for the moving interface of two-phase flow is as follows:

$$\frac{\partial\phi}{\partial t}+\vec{u}\cdot\nabla\phi=\gamma\nabla\cdot[\varsigma_{IS}\nabla\phi-\phi(1-\phi)\frac{\nabla\phi}{|\nabla\phi|}] \tag{3}$$

where ρ is the slurry density, $\vec{u}$ is the velocity field, ϕ is the level set variable, p is the pressure, γ is the Reinitialization parameter, ς_{IS} is the Control interface thickness parameter, μ is the dynamic viscosity, $\vec{g}$ is the acceleration of gravity, $\vec{F}$ is the Volume force of fluid.

3.1 Model of grout penetration in two-dimensional intersected fractures

3.1.1 Establishment of two-dimensional intersected fracture model

Considering the relative position, width, and angle of fracture in the fractured rock mass, the influence of time-varying characteristics of viscosity, the width of fracture and the injection position on the diffusion process are simulated. The intersected fracture model is established by simplifying the practical fracture distribution, and the model is shown in Fig 3. The model consists of a main fracture and two branch fractures. The length and width of the main fracture are 3 m and 3 cm, respectively. The length and width of the branch fracture 1 are 2 m and 2 cm, respectively, which intersects the main fracture at 1 m from the left end. The length and width of the branch fracture 2 are 2 m and 1 cm, respectively, which intersects the main fracture at 1 m from the right end. The two branch fractures are parallel with each other and the angle between the main and branch fractures is 60 degrees. To facilitate calculation, proper fillet treatment is performed at the intersection of cracks. The model has six ports as a, b, c, d, e and f as the model inlet or outlet. Under different situations, the boundary conditions of each port are different. A constant head is set for the outlet boundary, where the pressure is the same as the initial water pressure in the model. Other boundaries of the model are taken as impermeable.

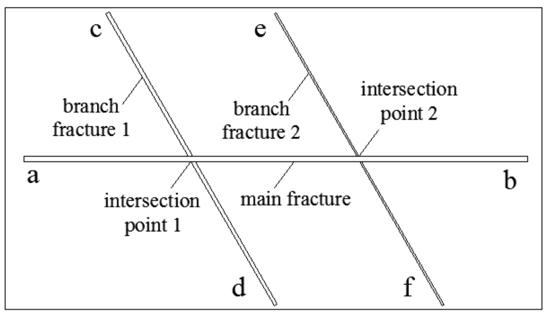

Figure 3: Model of two-dimensional intersected fractures for numerical simulation

3.1.2 Model parameters of two-dimensional intersected fractures

Water cement ratio of cement slurry, cement-water glass slurry and cement-water glass slurry with retarder is 1:1. The volume ratio of cement-water glass slurry without retarder is 1:1, whereas the volume ratio of cement-water glass slurry with retarder is 2:1. Normally, the values of these basic model parameters are chosen according to Tab. 2 (the test time is far shorter than that the gelling time of cement slurry, so the viscosity is assumed to be a constant value).

Table 2: Model parameters used for grouting simulation

Grout type	Grouting rate (m/s)	Hydrostatic pressure (Pa)	Outflow Boundary (Pa)	Slurry density (kg/m3)	Slurry viscosity (Pa·s)
Cement slurry	0.1	100	100	1490	0.018
Cement-water glass slurry	0.1	20000	20000	1400	$0.00240703t^3-0.05890892t^2+1.14539383t-2.86461943$
Cement-water glass slurry with retarder	0.1	20000	20000	1400	$0.00000096t^3-0.00078901t^2+0.26763018t+2.08222155$

3.2 Principle of grout penetration in intersected fractures under hydrostatic condition

3.2.1 Grouting condition

With varying location for grout injection, six types of grouting situations can be obtained, as given in Tab. 3.

Table 3: Six types of grouting conditions

Case 1	Case 2	Case 3	Case 4	Case 5	Case 6
a is the inlet and the rest are outlets.	b is the inlet and the rest are outlets.	c is the inlet and the rest are outlets.	d is the inlet and the rest are outlets.	e is the inlet and the rest are outlets.	f is the inlet and the rest are outlets

3.2.2 Numerical simulation of grout penetration

Grout penetration morphology

Cement slurry, cement-water glass slurry and cement-water glass slurry with retarder are not affected by hydrostatic water, and the slurry can be considered as uniform diffusion along the fracture. The penetration morphology of cement slurry, cement-water glass slurry and cement-water glass slurry with retarder is similar in the two-dimensional intersected fractures model, so the penetration morphology of cement slurry in hydrostatic water is given as an example. The diffusion range of slurry is mainly determined by injection rate under hydrostatic condition. Four typical situations are used for demonstrating the morphology of grout penetration, as shown in Fig. 4, including slurry injection, slurry diffusion reaching point 1, slurry diffusion reaching intersection point 2, and slurry filling with main fracture. The grout penetration morphology is expressed by the volume fraction ratio between slurry and water.

The diffusion distance of slurry and the time required to fill the whole intersected fracture model are affected by the injection rate and the width of fractures at the inlet. For the same kind of slurry, the smaller the fracture width is, the longer it takes for the slurry to fill the whole intersected fracture model.

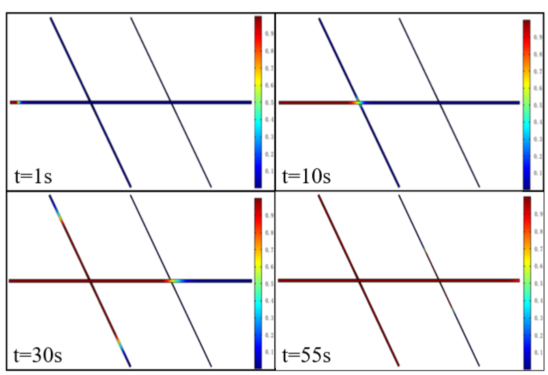

Figure 4: Cement slurry penetration morphology with time

Change of grouting pressure distribution

To analyze the mechanism of grout penetration in intersected fractures under different grouting conditions, pressure probes were set at the slurry entry, intersection point 1 and intersection point 2. The pressure variation curve at each probe is shown in Fig. 5. The variation patterns of Case 3 are like that of Case 4, and Case 5 is similar to Case 6, so only Case 3 and 5 are shown below.

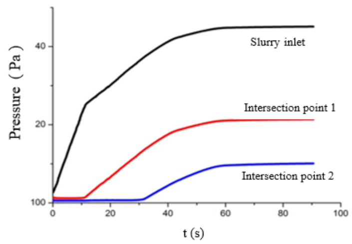

Case 1

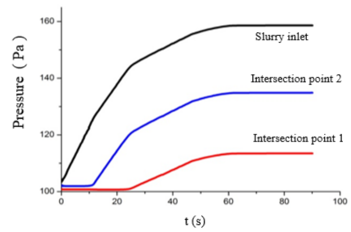

Case 2

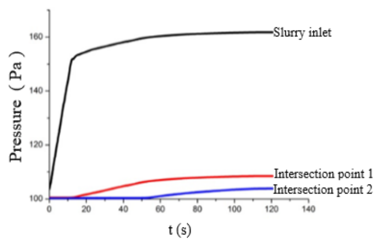

Case 3

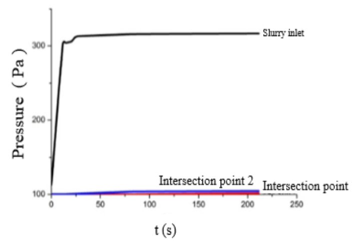

Case 5

(a) Pressure curve of cement slurry

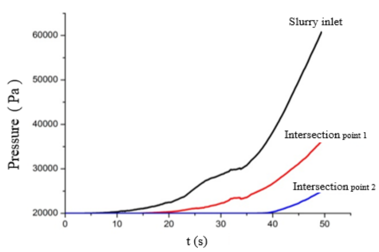

Case 1

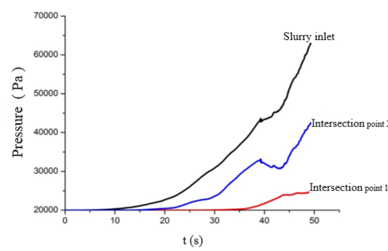

Case 2

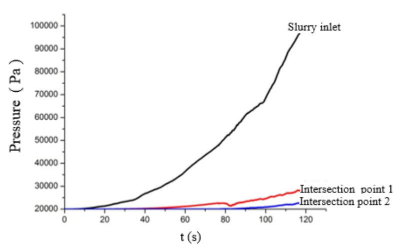

Case 3

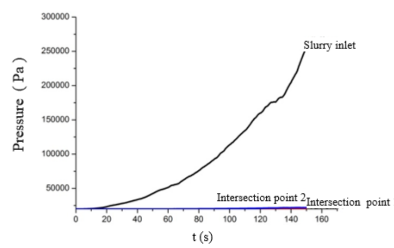

Case 5

(b) Pressure curve of cement-water glass slurry

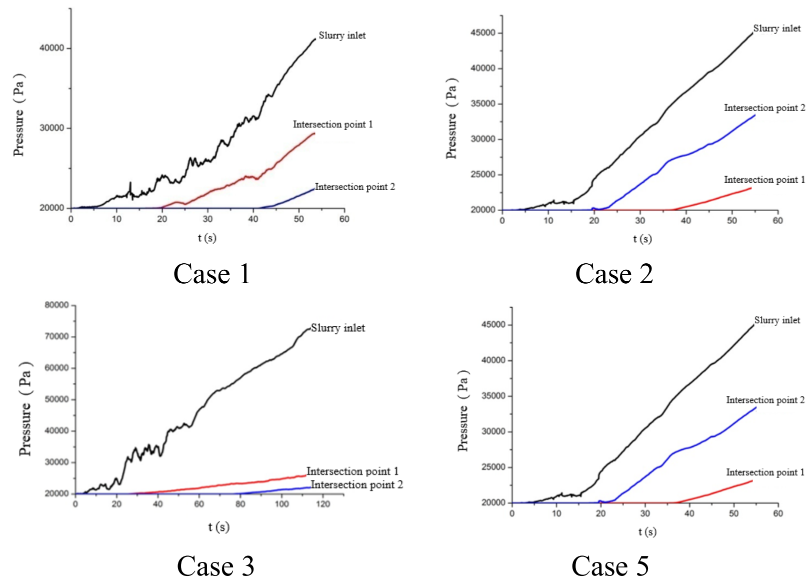

(c) Pressure curve of cement-water glass slurry with retarder

Figure 5: Curve of pressure change with time

Based analysis of pressure curves under different grouting conditions, it can be known that:

1) When the slurry enters the model, the pressure distribution in the model is mainly correlated to the inlet distance. At any time, the pressure at the inlet is the maximum, the closer to the inlet the higher the pressure, and the farther from the inlet the lower the pressure. The pressure must be more than or equal to the hydrostatic pressure.

2) According to pressure curve obtained from the model probe and the corresponding grout penetration morphology, it is found that the pressure variation is closely related to the slurry diffusion range. The grouting pressure of cement slurry is obviously affected by the branch fracture of the intersected fracture model, and the pressure variation curve can be divided into several stages, whereas the pressure curve corresponding to cement-water glass slurry with time-varying viscosity is less affected by the branch fracture. This indicates that variation of pressure curve during grouting is affected by the slurry viscosity, and the degree of impact is becoming lower with higher rate of rise of the slurry viscosity.

3) Under the same injection rate, the pressure patterns at each entry point and intersection point varies with varying conditions. When the inlet is in the main fracture (condition 1, 2), the grouting pressure increases slowly, the final grouting pressure is low, and the pressure difference between inlet and intersection point is small after the main fracture is filled with grout. When the inlet is in the branch fracture (condition 3, 5), the grouting pressure increases faster, and the final grouting pressure is higher. The results show that the slurry diffusion is greatly affected by the inlet location: when the inlet is in the main fracture, the pressure at each intersection point is relatively higher, and the slurry can fill branch fractures with good effect. When the inlet is in the branch fracture, the pressure at each intersection point is low though the pressure at the inlet is high, so the filling effect

regarding the main fracture and adjacent branch fracture is not good. Regarding the pressure curve, it is found that the pressure difference between inlet and intersection point is more significant when grout like cement-water glass with time varying viscosity is used as grouting material compared with that of cement slurry.

4) At the same stage, the pressure variation curve at the same position has an upward trend with time increasing, and the slope of the pressure curve is increasing. As pressure change is closely correlated with the time-varying viscosity of grout, the viscosity of cement-water glass slurry would increase gradually with time, leading to pressure increasing exponentially. However, at the same stage, the viscosity of cement slurry is almost unchanged, so the pressure increases linearly. According to numerical simulation, for most of the time, the rate of pressure rise of each slurry material at the same position of the model satisfies the following relationship: cement slurry<cement-water glass slurry<cement-water glass slurry with retarder.

(3) Analysis of grouting pressure

The variation curve of grouting pressure is shown in Fig. 6, which is obtained by collecting and processing the grouting pressure data under various conditions. Similarly, as Case 3 resembles Case 4, Case 5 resembles Case 6, so there is only one Case 3 and Case 5 are shown below.

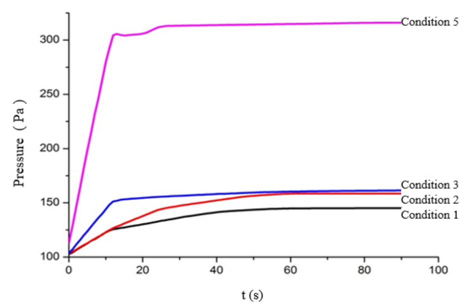

(a) Cement slurry

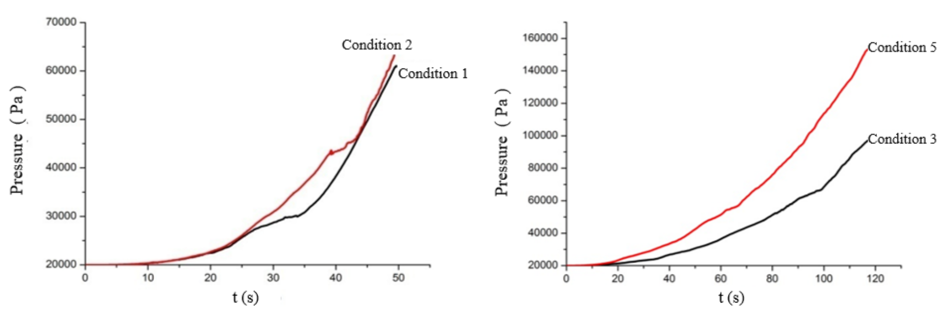

(b) Cement-water glass slurry

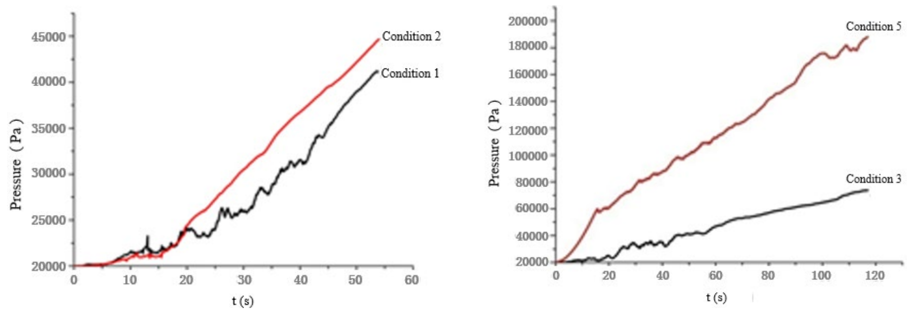

(c) Cement-water glass slurry with retarder

Figure 6: Curve of grouting pressure change

For grouting time less than 10 s, before grout front reaching the intersection point between the main fracture and branch fracture, and the rate of rise of the grouting pressure is mainly influenced by the width of the fracture at slurry inlet. For both Case 1 and Case 2, their slurry inlet is the main fracture, so the rate of rise of grouting pressure is the same. For Case 5, the fracture width of slurry inlet is the smallest, so the rate of rise of grouting pressure is the largest. Under the same injection rate, the grouting pressure increases with decreasing fracture width, and the rate of rise of grouting pressure under Case 5 can be twice as high as that under Case 1.

The variation pattern of injection pressure during grouting is related to the distribution of fractures. Comparison between Case 1 and Case 2, we know that their widths of branch fractures are different, and the corresponding variation curves of grouting pressure are different. For Cases 1 and 2, the rate of pressure rise decreases after the grout front reaching the intersection point. When the slurry front arrives at the first intersection point, the rate of rise of grouting pressure in Case 1 decreases greatly and the final grouting pressure is lower than that in Case 2, as the width of the branch fracture in Case 1 is larger than that in Case 2. In Cases 3 and 5, when the slurry diffuses from the branch fracture to the intersection point, the rate of rise of the grouting pressure is greatly reduced, and the grouting pressure tends to be stable, as the width of the main fracture is larger than that of the branch fracture.

4 Numerical investigation of grout penetration in three-dimensional intersected fractures

4.1 Model of grout penetration in three-dimensional intersected fractures

4.1.1 Model of three-dimensional intersected fractures

The model consists of a main fracture and two branch fractures. The length and width of the main fracture are 3 m and its thickness is 3 cm. The length and thickness of the branch fracture 1 are 2 m and 2 cm, respectively, and it intersects the main fracture at 1 m from the left end. The length and thickness of the branch fracture 2 are 2 m and 1 cm, respectively, and it intersects the main fracture at 1 m from the right end. The two branch fractures are parallel to each other, rotating 60 degrees clockwise from the main fracture. To facilitate calculation, proper fillet treatment is performed at the crack intersections.

The model is shown in Fig. 7. In the model, a grouting hole with radius of 2 cm is set at the center of the main fracture, and two ends of the main fracture and individual branch fracture are set as the inflow or outflow of grout and groundwater. Under different conditions, the boundary conditions are different. A constant head is set for the outlet boundary and the pressure is the same as the initial water pressure. The other boundary of the model is impermeable.

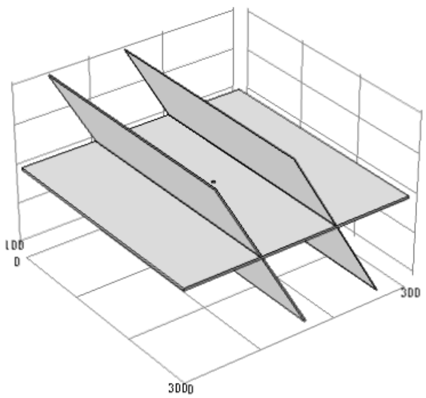

(a) Three-dimensional model

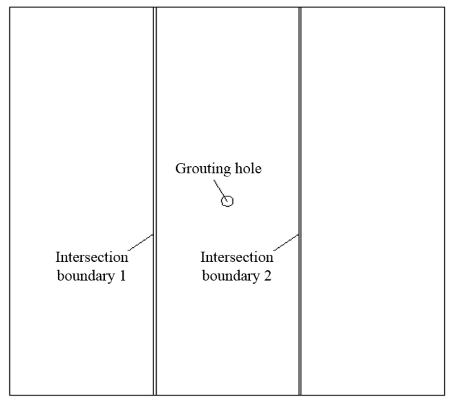

(b) Vertical view of the main fracture surface

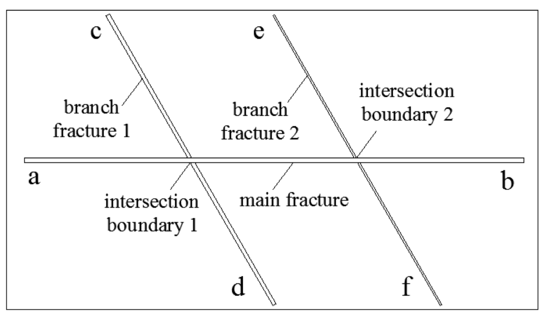

(c) Front view of the model

Figure 7: Three-dimensional model of intersected fractures

4.1.2 Model parameters of three-dimensional intersected fractures

Water cement ratio of cement slurry, cement-water glass slurry and cement-water glass slurry with retarder is 1:1. The volume ratio of cement-water glass slurry without retarder is 1:1, the volume ratio of cement-water glass slurry with retarder is 2: 1. In the following discussion, the values of basic model parameters are chosen from Tab. 4 (the test time is far shorter than that the gelling time of cement slurry, so the viscosity is assumed to be a constant value). The injection rate of grout is 0.6 m/s.

Table 4: Model parameters used for grouting simulation

Grout type	Grouting rate (m/s)	Hydrostatic pressure (Pa)	Outflow boundary (Pa)	Slurry density (kg/m^3)	Slurry viscosity (Pa·s)
Cement slurry	0.6	100	100	1490	0.018
Cement-water glass slurry	0.6	20000	20000	1400	$0.00240703t^3-0.05890892t^2+1.14539383t-2.86461943$
Cement-water glass slurry with retarder	0.6	20000	20000	1400	$0.00000096t^3-0.00078901t^2+0.26763018t+2.08222155$

4.2 Principle of grout penetration in intersected fractures under hydrostatic condition

4.2.1 Numerical simulation of grout penetration

Grout penetration morphology

During the grouting process, assuming that cement slurry, cement-water glass slurry and cement-water glass slurry with retarder are not affected by hydrostatic water, and the slurry diffusion within fractures can be considered to be uniform.

The patterns of grout penetration at t=1 s, t=80 s and other time are used for characterizing the dynamic diffusion process of grout, as shown in Fig. 8. The grout penetration morphology is expressed by the volume fraction ratio between slurry and water.

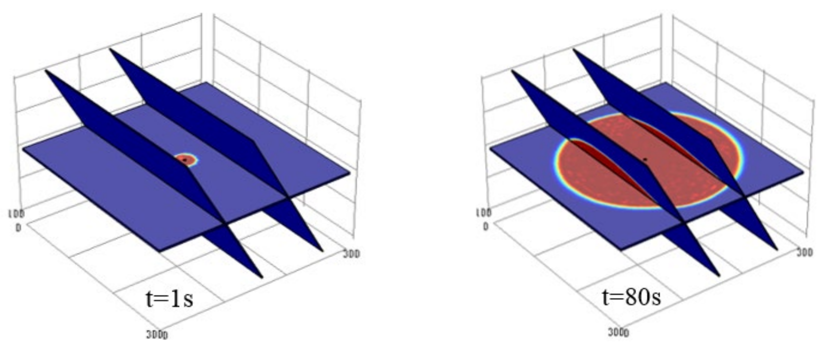

(a) Cement slurry penetration morphology

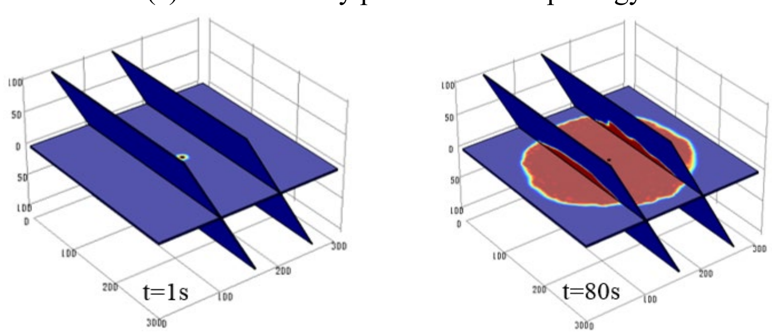

(b) Cement-water glass slurry penetration morphology

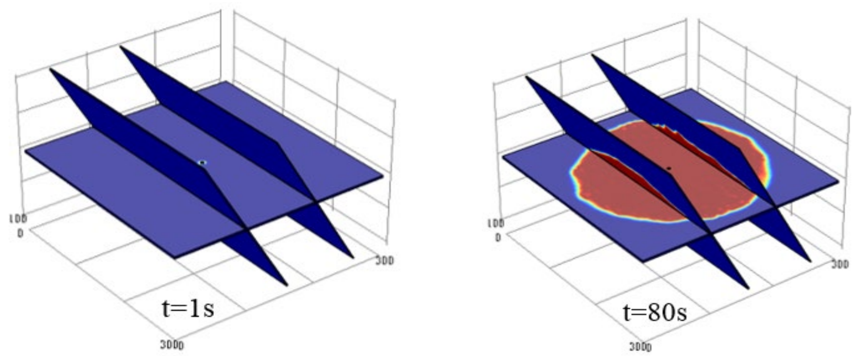

(c) Cement-water glass slurry with retarder penetration morphology

Figure 8: Slurry penetration morphology

It is found that when the grouting material enters the model, the penetration morphology of the slurry is related to the time-varying viscosity of grouting material itself. For the cement slurry whose viscosity changes slowly with time, the slurry penetration morphology is regular in both main fracture and branch fractures, and the transition area between slurry mixture and water is stable. For the cement-water glass slurry whose viscosity changes rapidly with time, the slurry penetration morphology is irregular in both main fracture and branch fractures, and the transition area between slurry mixture and water is distorted.

Distribution of grouting pressure

During the process of slurry diffusion, the pressure field changes continuously. The pressure field at t=1 s and t=80 s is selected to characterize the variation process of pressure field, as shown in Fig. 9.

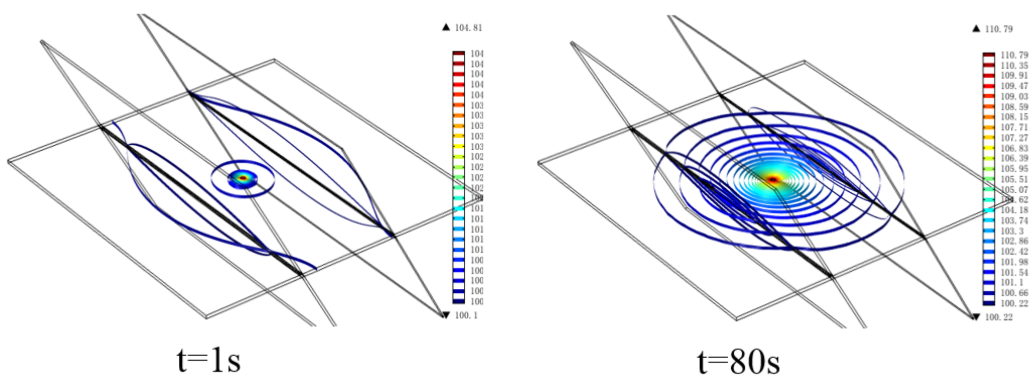

(a) Cement slurry

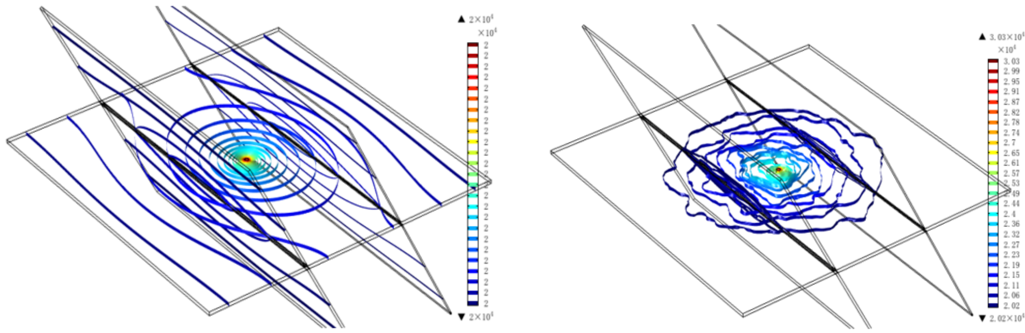

t=1s t=80s

(b) Cement-water glass slurry

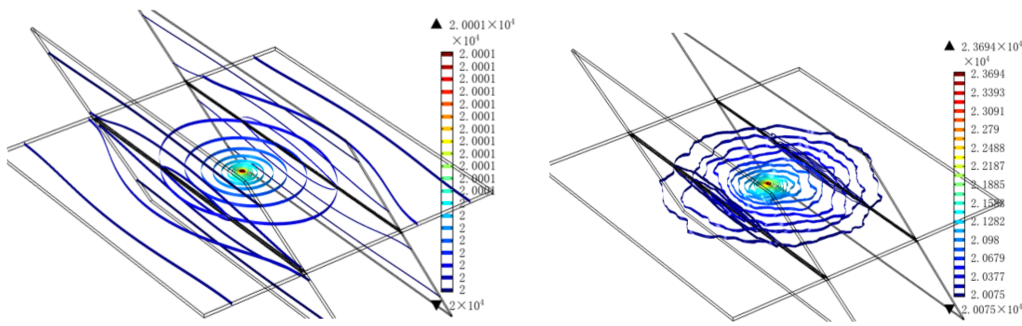

t=1s t=80s

(c) Cement-water glass slurry with retarder

Figure 9: Pressure field distribution based on numerical simulation

When the slurry enters the model, the pressure distribution of the model is mainly related to the distance between the inlet and the grout front and the time-varying viscosity of slurry. At any time, the pressure at the inlet is the maximum, the closer to the inlet, the greater the pressure, and vice versa. The pressure distribution on the surface of the main fracture is symmetric about injection hole. For the cement slurry whose viscosity changes slowly with time, the pressure distribution is uniform with smooth iso-surfaces. For the cement-water glass slurry whose viscosity changes rapidly with time, the pressure distribution in the model is not uniform, and the pressure iso-surface is wavy. Retarder can effectively reduce the growth rate of slurry viscosity, and the pressure distribution of cement-water glass slurry with retarder is more uniform.

When the slurry reaches the intersected surface, the distribution of pressure iso-surface in the main fracture changes due to the effect of flow diversion from branch fracture. The larger the width of the branch fracture is, the more obvious the pressure distribution is in the main fracture. Compared with the cement slurry, the time-varying viscosity of grout as cement-water glass slurry is less affected by the branch fracture.

Grout penetration morphology in branch fractures

To analyze the influence of different fracture width on the grout penetration morphology in the branch fracture, the grout penetration morphology in branch fractures at t=32 s and t=80 s are used for comparative analysis, as shown in Fig. 10, where the left side is branch fracture 1, and the right side is branch fracture 2.

The range and velocity of diffusion slurry in the branch fracture are affected by the fracture width. The wider the fracture width, the faster the diffusion of slurry and the wider the range of slurry diffusion. Compared with the cement slurry, the time-varying viscosity of the cement-water glass is affected by its time-varying viscosity, and the grout penetration in the branch fracture has no obvious patterns.

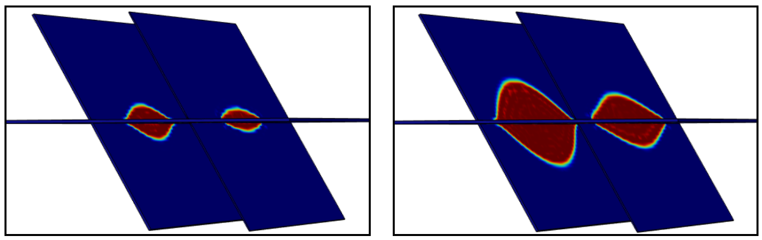

t=32 s t=80 s

(a) Cement slurry

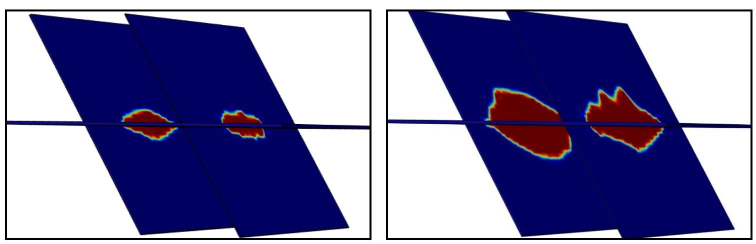

t=32 s t=80 s

(b) Cement-water glass slurry

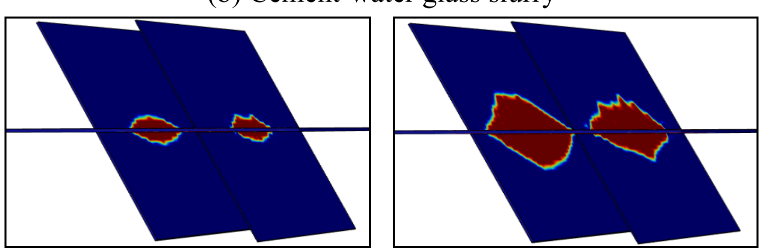

t=32 s t=80 s

(c) Cement-water glass slurry with retarder

Figure 10: Grout penetration morphology of branch fractures

Analysis of slurry distribution and pressure variation in intersected boundary

To analyze the diffusion rule of cement slurry at the intersected boundary, the pressure distribution of fracture boundary 1 and fracture boundary 2 and the distribution of the volume ratio between slurry and water in mixed area are compared and analyzed, as shown in Figs. 11 and 12.

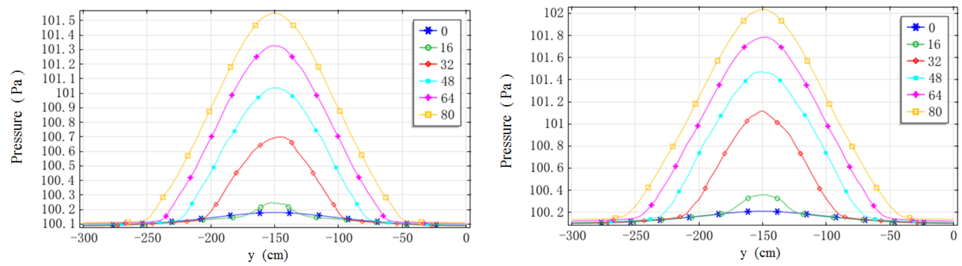

Intersected boundary 1 Intersected boundary 2

(a) Cement slurry

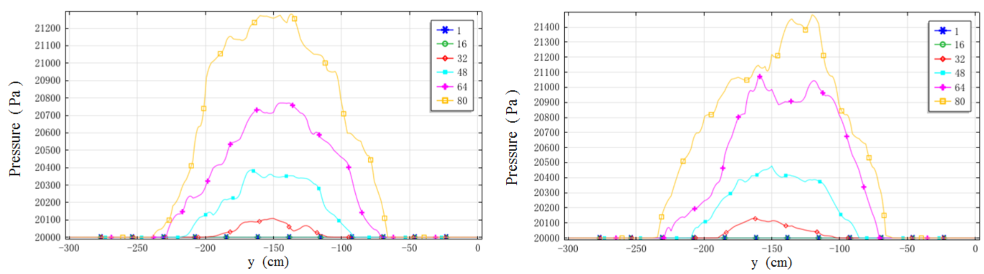

Intersected boundary 1 Intersected boundary 2

(b) Cement-water glass slurry

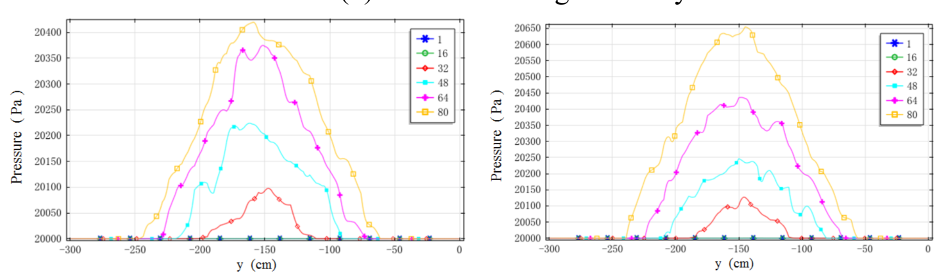

Intersected boundary 1 Intersected boundary 2

(c) Cement-water glass slurry with retarder

Figure 11: The pressure distribution of intersected boundary

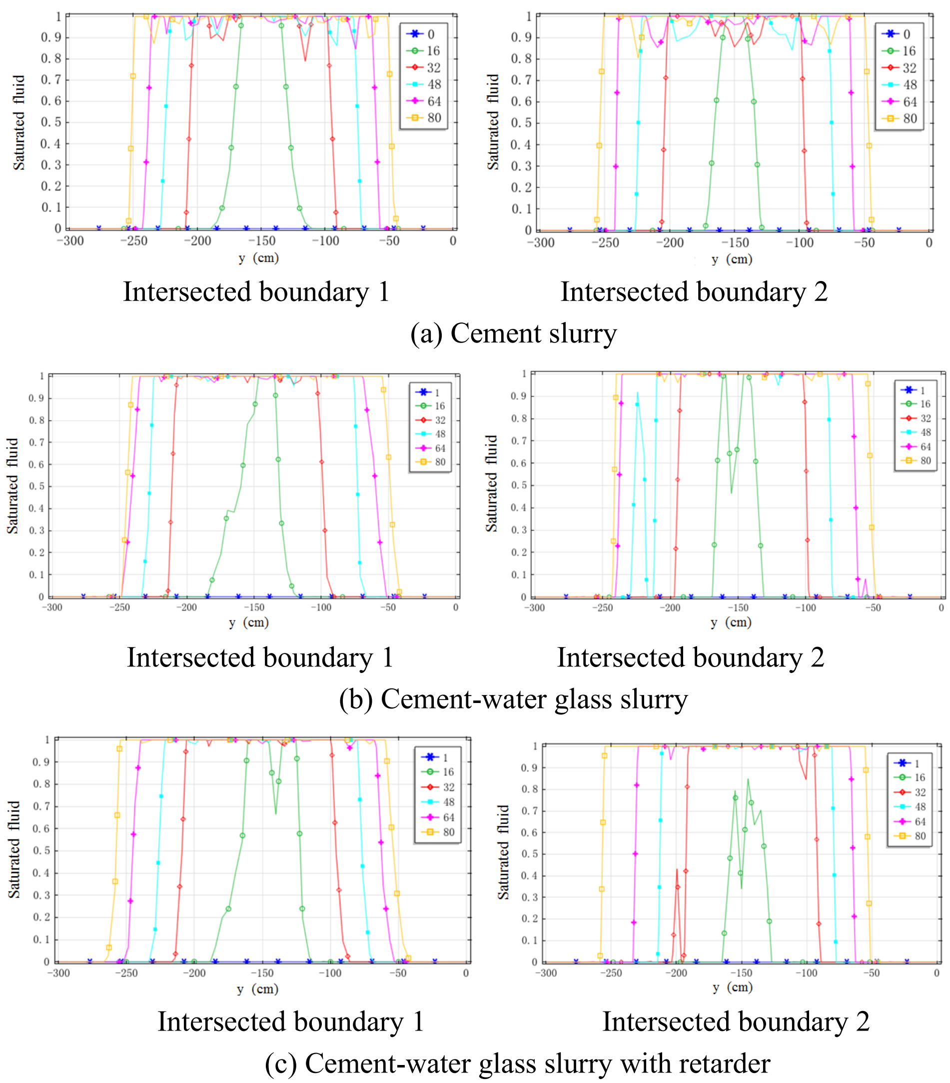

Figure 12: Distribution of volume ratio between slurry and water in the mixture zone

The variation of pressure distribution at the intersected boundary follows the variation patterns of the pressure field in the main fracture. For the cement slurry with slowly time-varying viscosity, and the variation patterns of pressure curve at the intersected boundary is smooth. For the cement-water glass slurry with rapidly time-varying viscosity, the variation patterns of pressure curve at the intersected boundary is wavy. At the same time, the pressure at intersected boundary 2 is slightly higher than that at intersected boundary 1. The faster the slurry viscosity increases, the more larger the pressure gap is, indicating that the resistance to slurry diffusion increases with decreasing width of branch fracture, and the groutability of branch fractures are becoming worse.

By comparing and analyzing the pressure distribution at the intersected boundary, the distribution of volume ratio of slurry and the grout penetration morphology, we found that the distribution patterns of slurry at the intersected boundary follows well that in main fracture. For cement slurry, the volume ratio distribution at intersected boundary 1 and intersected boundary 2 is almost the same. For the cement-water glass slurry with time-varying viscosity, the grout penetration morphology in the main fracture is irregular. Therefore, the pressure distribution curve at intersected boundary is not smooth, and there is a great difference between intersected boundary 1 and 2 regarding the volume ratio of slurry.

5 Discussion

Regarding the shortcomings in investigating the mechanism of grout penetration in intersected fractures, the following discussions are given to provide ideas and suggestions for future research:

(1) In underground engineering, the internal structure of fractured rock mass is complex and diverse. The size and direction of fracture, roughness, aperture and so on would greatly affect the patterns of grout penetration in fractures. Considering and quantifying those impact factors involved in slurry diffusion, we can develop a more practical fracture network. It is of great significance to develop grouting theory and conduct numerical simulation, and to explore physical principles and grouting effect.

(2) In the process of slurry diffusion, the flow of groundwater will dilute and flush the slurry. In numerical simulation, consideration of the interaction between slurry and water, and investigation of the influence of water on the physical and chemical properties of slurry, can play an important role in the accuracy of numerical simulation.

(3) For slurry flow, especially in the process of flow diversion, the pressure will be dissipated. As an important index for practical engineering grouting, it is of great significance to quantitatively analyze the distribution of pressure in process of slurry flow and to determine the reasonable range of slurry diffusion and the final grouting pressure.

6 Conclusions

In the present paper, cement slurry and fast-setting cement slurry are used, and the influence of retarder and time-varying viscosity are considered. The penetration mechanism and pressure distribution of cement-based slurry in intersected fractures during grouting are studied by establishing two and three-dimensional numerical models for grouting of intersected fracture under hydrostatic condition.

(1) Under a specific slurry flow rate, the grouting pressure and its rate of rise are related to the fracture width at the slurry inlet, the smaller the crack width, the faster the grouting pressure increases, and the higher the grouting pressure when the pressure variation becomes stable.

(2) The slurry diffusion range and the time required to fill the whole intersected fracture are affected by the injection rate and the width of fractures at the inlet. In terms of one specific type of slurry, the smaller the fracture width, the longer it will take for the slurry to fill the whole intersected fracture model.

(3) The grout penetration morphology, the distribution of pressure field and grouting pressure are related to the time-varying characteristics of slurry viscosity under hydrostatic environment. For cement slurry, the viscosity is almost unchanged and the

slurry penetration morphology is regular in main fracture and branch fractures, the pressure field is uniform, and the grouting pressure changes slowly with time. The grout penetration morphology and the distribution of pressure are apparently affected by the branch fractures. For time-varying properties of the cement-water glass slurry, the viscosity increases rapidly with time and the slurry penetration morphology is irregular in main fracture and branch fractures, the pressure field is not uniform, and the grouting pressure changes rapidly with time. The grout penetration morphology and the distribution of pressure are relatively less affected by the branch fractures.

(4) Retarder can effectively reduce the growth rate of slurry viscosity and increase the diffusion range of cement-water glass slurry. In practical application, the slurry gelling time can be controlled by adjusting its proportion in grout to control grouting and meet more engineering needs.

Acknowledgement: This work was financially supported by the Joint Funds of National Natural Science Foundation of China [Grant No. U1706223]; the National Key Research and Development Project (Grant No. 2016YFC0801600); the General Program of National Natural Science Foundation [Grant No. 51779133]; and the General Program of Shandong Province Natural Science Foundation [Grant No. ZR2018MEE047].

References

Amadei, B.; Savage, W. Z. (2001): An analytical solution for transient flow of Bingham viscoplastic materials in rock fractures. *International Journal of Rock Mechanics and Mining Sciences*, vol. 38, no. 2, pp. 285-296.

Baker, W. J. (1955): Flow in fissure formations. *4th proceeding of the World Petroleum Congress*, Rome, Section II, pp. 379-393.

Carter, T. G.; Dershowitz, W.; Shuttle, D. (2012): Improve methods of design for grouting fractured rock. *Grouting and Deep Mixing, Geotechnical Special Publications*, vol. 2, no. 28, pp. 1472-1483.

Dai, G.; Bird, R. B. (1981): Radial flow of a Bingham fluid between two fixed circular disks. *Journal of Non-Newtonian Fluid Mechanics*, vol. 8, no. 3, pp. 349-355.

Deere, D.; Lombardi, G. (1985): Grout slurries-thick of thin. *Issues in Dam Grouting, Proceedings of the Session Sponsored by the Geotechnical Engineering Division of American Society of Civil Engineers in Conjunction with the ASCE Convention in Denver*, Colorado, USA.

Eriksson, M.; Stille, H.; Andersson, J. (2000): Numerical calculaions for prediction of grout spread with account for filtration and varying aperture. *Tunnelling and Underground Space Technology*, vol. 15, no. 4, pp. 353-364.

Gothall, R.; Stille, H. (2009): Fracture dilation during grouting. *Tunnelling and Underground Space Technology Incorporating Trenchless Technology Research*, vol. 24, no. 2, pp. 126-135.

Gothall, R.; Stille, H. (2010): Fracture-fracture interaction during grouting. *Tunneling and Underground Space Technology*, vol. 25, no. 3, pp. 199-204.

Hao, M.; Wang, F.; Li, X. (2017): Numerical and experimental studies of diffusion law of grouting with expansible polymer. *Journal of Materials in Civil Engineering*, vol. 30, no. 2, pp. 04017290.

Hässler, L.; Håkansson, U.; Stille, H. (1992): Computer-simulated flow of grouts in jointed rock. *Tunnelling and Underground Space Technology*, vol. 7, no. 4, pp. 441-446.

Kim, H. M.; Lee, J. W.; Yazdani, M. (2018): Coupled viscous fluid flow and joint deformation analysis for grout injection in a rock joint. *Rock Mechanics and Rock Engineering*, vol. 51, no. 2, pp. 627-638.

Li, H. M.; Huang, X. G.; Liang, W. M. (2008): Study on the diffusion law of permeation grouting in oval fissure. *Journal of Henan Polytechnic University (Natural Science)*, vol. 27, no. 5, pp. 573-576.

Li, S. C.; Zhang, X.; Zhang, Q. S. (2011): Research on mechanism of grout diffusion of dynamic grouting and plugging method in water inrush of underground engineering. *Chinese Journal of Rock Mechanics and Engineering*, vol. 30, no. 12, pp. 2377-2396.

Ping, L. P.; Ming, Z. Y.; Gui, H. J.; Min, L. A. (2006): Two-dimensional numerical simulation of grouting in random fractured rock mass. *Journal of Hohai University Natural Sciences*, vol. 34, no. 3, pp. 295-298.

Wallner, M. (1976): Propagation of sedimentation stable cement pastes in jointed rock. *Rock Mechanics and Waterways Construction*, no. 2, pp. 49-165.

Wang, Q.; Feng, Z. Q.; Wang, L. X. (2016): Numerical analysis of grouting radius and grout quantity in fractured rock mass. *Journal of China Coal Society*, vol. 41, no. 10, pp. 2588-2595.

Yang, M. J. (2000): *Mechanism of Grout Penetrating in Stochastic Fractured Rock Mass and Its Stability Analysis After Reinforcement*. China University of Mining and Technology.

Yang, M. J.; He, Y. N.; Chen, M. X. (2001): Law of grouting penetrating through fracture network of rock mass. *Shuili Xuebao*, no. 7, pp. 41-46.

Yang, P.; Sun, X. Q. (2015): Single fracture grouting numerical simulation based on fracture roughness in hydrodynamic environment. *Electronic Journal of Geotechnical Engineering*, vol. 20, no. 1, pp. 59-67.

Zhang, Q. S.; Zhang, L. Z.; Liu, R. T. (2015): Laboratory experimental study of cement-silicate slurry diffusion law of crack grouting with dynamic water. *Rock and Soil Mechanics*, vol. 36, no. 8, pp. 2159-2168.

Zhao, P.; Zhang, Q. S.; Zheng, D. Z. (2016): Research and application of influence mechanism about phosphate retarder for cement-based fast curing grouts. *Bulletin of the Chinese Ceramic Society*, vol. 35, no. 4, pp. 989-994.